Multitimescale Reliability Evaluation of DC-Link Capacitor Banks in Metro Traction Drive System

Yao, Bo; Ge, Xinglai; Wang, Huimin; Wang, Haoran; Zhou, Dao; Gou, Bin

Published in:
IEEE Transactions on Transportation Electrification

DOI (link to publication from Publisher):
10.1109/TTE.2020.2974182

Publication date:
2020

Document Version
Accepted author manuscript, peer reviewed version

IEEE POWER ELECTRONICS REGULAR PAPER/LETTER/CORRESPONDENCE

Multi-Timescale Reliability Evaluation of DC-link Capacitor Banks in Metro Traction Drive System

Bo Yao, *Student Member, IEEE*, Xinglai Ge, *Member, IEEE*, Huimin Wang, *Student Member, IEEE*, Haoran Wang, *Member, IEEE*, Dao Zhou, *Senior Member, IEEE*, and Bin Gou, *Member, IEEE*

***Abstract*- The reliability of DC-link capacitors in urban rail transit is considered as a major challenge because of significant maintenance impact. In this paper, the DC-link capacitor reliability is researched in metro traction drive system. In the small timescale of control level, the current harmonics of multiple operating conditions and different control methods in the DC-link capacitor are discussed. The power loss is simulated by the capacitor harmonics of current and equivalent series resistance (ESR) in multi-operating conditions. Considering electro-thermal coupling, the time-ordered and continuity of thermal stress are analyzed to evaluate the hot spot temperature dynamic conformed to the reality. Combining with the analysis of electrical stress and thermal stress, a multi-timescale capacitor reliability evaluation method is proposed. It is divided into four steps: the discrete small timescale, the single route timescale, the daily operation timescale and the whole lifetime cycle. In the different timescales, the lifetime distribution changes with the dynamics of the complex mission profiles, so as to estimate the lifetime bottleneck of the DC-link capacitor banks with different control methods by the Weibull distribution. In addition, experimental validation is provided to verify the accuracy of the proposed method.**

***Index Terms*--DC-link capacitor, multi-timescale, reliability, metro traction drive system, Weibull distribution.**

I. INTRODUCTION

Passive components typically require a lifetime cycle more than a decade or even decades [1], which demands a carefully designed lifetime and failure rate at the beginning of device selection [2]. Capacitors are considered as one of the most vulnerable components in power electronic systems [3], and the reliability of DC-link capacitors has increasingly become a concerning issue in the traction drive system [4].

In recent years, the lifetime evaluation methods for capacitors have been proposed in the literatures. Among them, the mathematical models of aluminum electrolytic capacitors (Al-Cap) and Film capacitor (Film-Cap) lifetime are given and the failure mechanism of the DC-link capacitor is analyzed in [5]. For the Al-Cap, the calculation method of the capacitance loss of the Al-Cap is proposed based on the experimental data [6]. In [7], the corresponding relationship between the electro-thermal stress and the aging of the capacitor is established according to the mechanism of the Al-Cap capacitance loss. Due to potential reliability improvement that leads to reduction of cost, the Film-Cap have gradually been applied [8], [9]. In regard to Film-Cap, the nonlinear variation of the capacitor is studied by accelerated aging test in [10]. The data analysis of the nonlinear variation law using the Poisson distribution model is studied for the lifetime evaluation of the Film-Cap in [11]. As the system complexity increases, the impact of the mission profile on the lifetime of the capacitor cannot be ignored. In [12], according to the imbalance of grid voltage, the capacitor lifetime estimation method based on nonlinear cumulative damage is presented. In [13], considering the mission profile of wind speed and ambient temperature, the aging process and equivalent series resistance (ESR) of the capacitor are analyzed, and an analysis method for evaluating the reliability of the capacitor banks is proposed in [14]. However, the existing literatures only have relatively gradual and independent mission profile in research systems, such as the wind speed in the wind power system, the light intensity in the photovoltaic system, and the ambient temperature [15]. In the metro traction drive system, due to the fast startup and shutdown operation among the short distance stations on the route [16], the mission profile includes different line speeds, slopes, the long-term changes in passenger flow and ambient temperature. Combining the complex dynamics of short-term and long-term mission profiles with the actual capacitor load curve in the multi-operating condition system, and correctly applying the electrical parameters of the traction system to the capacitor lifetime model is still a huge challenge.

Thermal stress is a key issue in capacitor wear, which leads to shortened life cycles [5]. The research on thermal stress analysis about capacitor is mainly divided into mathematical models and physical models. In terms of mathematical models, a model for quickly estimating the hot spot temperature of the single capacitor is established in [17]. For applications with multiple capacitors, the thermal stress of the capacitor banks is discussed by establishing a convective and radiative heat transfer model in [18]. The nonlinear mathematical model of the capacitor banks is further proposed, and the thermal stress modeling calculation is performed by establishing a simple RC thermal network [19]. A temperature monitoring method for a DC link capacitor is proposed to obtain thermal stress in [20]. In terms of the physical model, a capacitor thermal network model is established by the thermal parameters of the lateral structure of the capacitor according to the mounting boundary

This work was supported by the Project Supported by High-Speed Railway Joint Funds of the National Natural Science Foundation of China (U1934204) and the Project Supported by National Natural Science Foundation of China (51677156, 61733015). (*Corresponding author: Xinglai Ge*).

X Ge, B. Yao, H. Wang, and B. Gou are with the Ministry of Education Key Laboratory of Magnetic Suspension Technology and Maglev Vehicle, Southwest Jiaotong University, Chengdu 610031, China (e-mail: yaobo1666@my.swjtu.edu.cn; wanghuimin@my.swjtu.edu.cn; xlgee@163.com; bingo57350@126.com).

H. Wang and D. Zhou are with the Department of Energy Technology, Aalborg University, Aalborg 9220, Denmark (e-mail: hao@et.aau.dk; zda@et.aau.dk).

This article has been accepted for publication in a future issue of this journal, but has not been fully edited. Content may change prior to final publication. Citation information: DOI 10.1109/TTE.2020.2974182, IEEE Transactions on Transportation Electrification

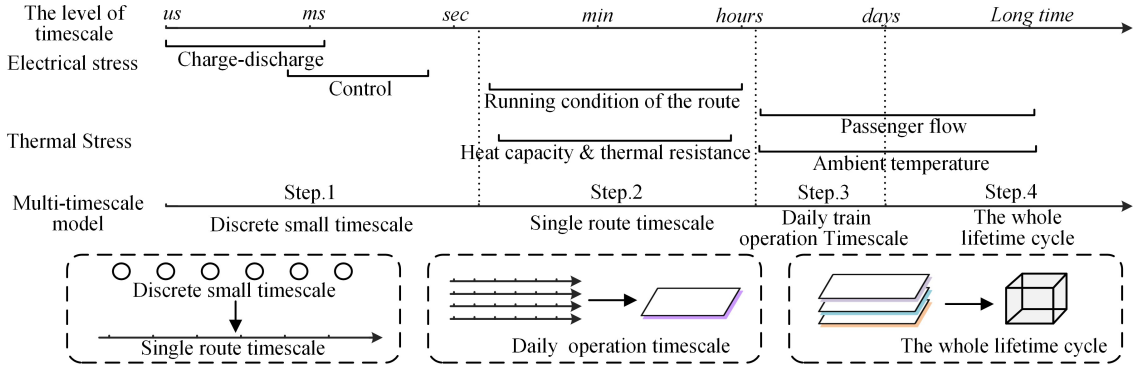

Fig. 1. Research strategies of multiple timescales in the metro traction drive system

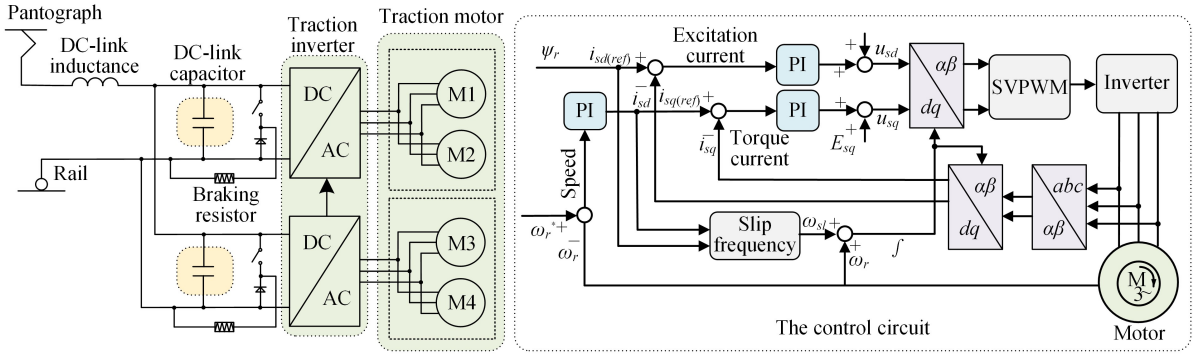

Fig. 2. Schematic diagram of metro traction drive system

conditions of the capacitor [21]. In [22], the thermal model of the capacitor is established by calculating the electrical conductivity of the electrolytic capacitors with different boundary conditions. It is also an effective way to analyze the temperature distribution of the capacitor by establishing a heat transfer model through the finite element model [23]. The pseudo 3D thermal model is further established by the material geometry and thermal performance parameters, but due to the complex model structure, the operation speed has constraints [24]. When analyzing the thermal stress of the DC-link capacitor, the existing literatures usually discusses the hot spot temperature through an independent mathematical model or physical model. Because of the multi-operating condition and complex mission profiles in the traction system, the electrical signal dynamics of the DC-link capacitor is rapid and random. It is necessary to combine the capacitor mathematical model with the physical model to consider the time-ordered and continuity of the multi-time dynamic temperature distribution based on the electro-thermal coupling model.

In addition, the concept of timescale has been initially applied to the related research of energy management and power device reliability. Multi-timescale model is established on wind speed and wind power prediction problems [25], [26]. Physical fatigue caused by material parameters is quantified by a small timescale model [27]. The reliability of the converter system is evaluated by dividing into multiple modeling levels and taking into account the thermo-dynamic timescale [28].

As shown in Fig. 1, the timescale methods are introduced into the capacitors reliability research. It can be seen that the electro-thermal interference in the metro traction drive system has different timing instances ranging from microseconds (charging-discharging and control) to more than one day (ambient temperature and passenger flow), which is hardly described with a single timescale analytical model. In order to solve the problem of analyzing the electric-thermal coupling relationship and solve the reliability model of DC-link capacitors banks under multi-operating conditions and complex mission profiles in metro traction drive system, this paper presents a multi-timescale reliability evaluation model to obtain the DC-link capacitor lifetime bottleneck. In the beginning, the reliability index of the discrete small timescale is obtained by the electro-thermal coupling model. Then, the mission profile at the running line level is introduced to obtain the reliability distribution of the single route cycle. Furthermore, the influence of changes in passenger flow and ambient temperature on the reliability change is considered in daily operation timescale and complete lifetime cycle.

In Section II, the electrical model and physical model of the DC-link capacitor are introduced. In Section III, combined with multiple timescales electro-thermal stress coupling, the time-ordered and continuous of temperature dynamics are analyzed. In Section IV, a multi-timescale lifetime evaluation model of the DC-link capacitor banks and experimental verification are presented.

This article has been accepted for publication in a future issue of this journal, but has not been fully edited. Content may change prior to final publication. Citation information: DOI 10.1109/TTE.2020.2974182, IEEE Transactions on Transportation Electrification

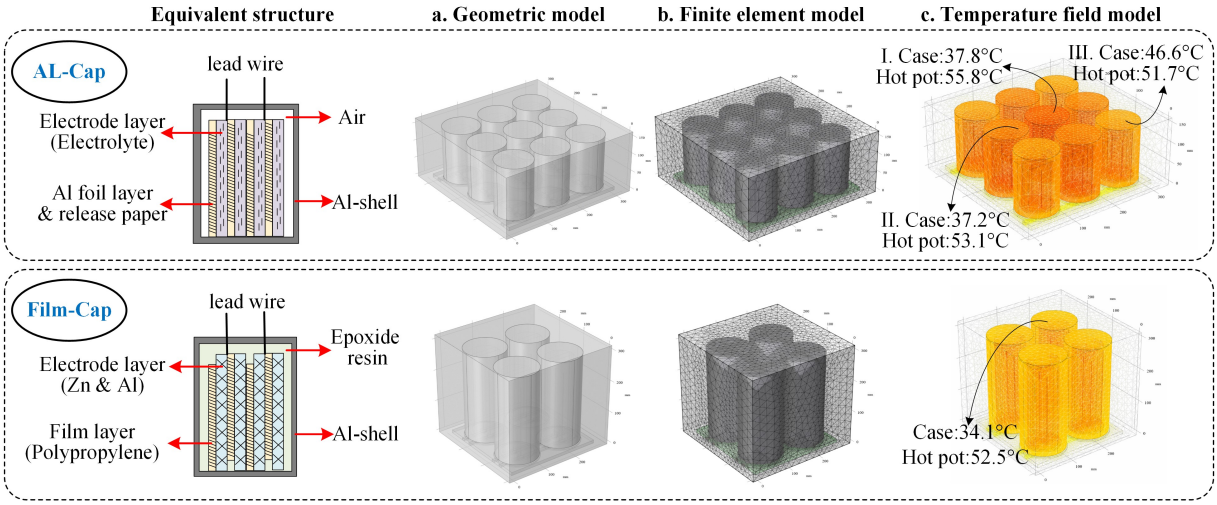

Fig. 3. Multi-physics finite element analysis of AL-Cap and Film-Cap

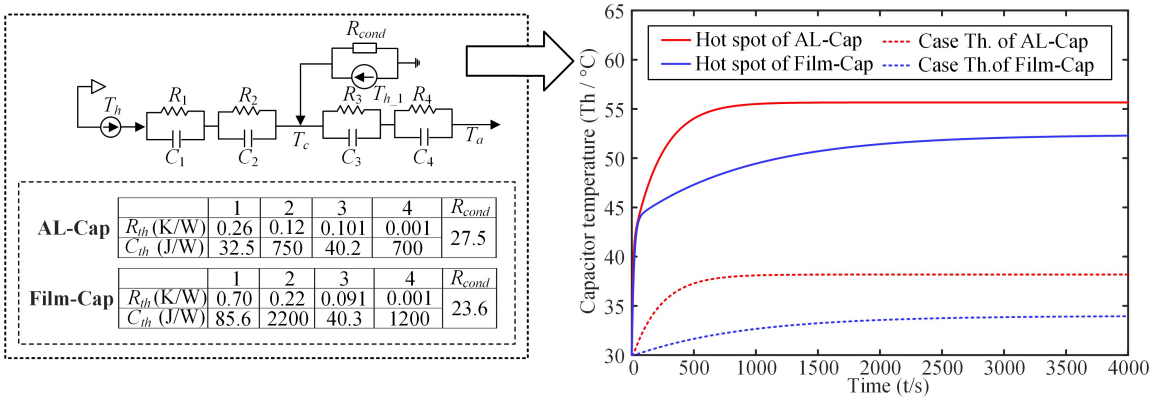

		1	2	3	4	R_{cond}
AL-Cap	R_{th} (K/W)	0.26	0.12	0.101	0.001	27.5
	C_{th} (J/W)	32.5	750	40.2	700	
Film-Cap	R_{th} (K/W)	0.70	0.22	0.091	0.001	23.6
	C_{th} (J/W)	85.6	2200	40.3	1200	

Fig. 4: Foster model and the case and hot spot temperature curve of DC-link capacitor

II. The Electrical and Physical Models

A. Electrical Model of the DC-link Capacitor

Fig. 2 shows the electrical model of the DC-link capacitor in the metro traction drive system. The transmission mode is realized by the DC link, in which the large-capacity capacitors are used to reduce DC-link voltage fluctuations and energy exchange. The control method adopts vector control based on field-orientation as well as the modulation method mainly uses SVPWM [29]. The sensors collect the signal of the DC-link voltage, stator current and speed. Meanwhile, it combines the traction control instruction and the vector control principle to obtain the modulation voltage instruction, and finally realizes the instruction control through the SVPWM modulation in the inverter.

B. Physical Model of the DC-link Capacitor

The capacitor thermal stress can be demonstrated by the case temperature and hot spot temperature in the DC-link capacitor. Based on the mathematical model, the AL-Cap and Film-Cap hot spot temperature T_h and the power loss P_{loss} are obtained as [5], [12]:

$$\begin{cases} T_h = T_a + \Delta T = T_a + R_{th} P_{loss} \\ P_{loss} = \sum_{i=1}^{n} \left[ESR(f_i) \times I_{rms}^2(f_i) \right] \end{cases} \quad (1)$$

where T_a and R_{th} are the ambient temperature and the equivalent thermal resistance. $ESR(f_i)$ and $I_{rms}(f_i)$ represent the ESR and the root mean square (RMS) value of the ripple current at frequency f_i, respectively.

In order to obtain the thermal network model parameters of the DC-link capacitor, the multi-physics coupling models of the AL-cap and the Film-Cap are established as shown in Fig. 3 [21], [22]. In Fig. 3(a), the material properties (including thermal conductivity, heat capacity, density, etc.) of the different layered structures of AL-cap and Film-Cap are considered in the geometry model. In Fig. 3(b), the finite element model is built by meshing. In Fig. 3(c), taking into account the series-parallel connection in the electro-thermal model, the different temperature of the AL-cap and the Film-Cap is monitored by setting the generated power loss P_{loss}.

Because the power loss P_{loss} is an irregular variable, there is the limit of computational capacity to the application of multi-physics modeling. In order to establish the quantitative relationship of fast calculation among the hot spot temperature

This article has been accepted for publication in a future issue of this journal, but has not been fully edited. Content may change prior to final publication. Citation information: DOI 10.1109/TTE.2020.2974182, IEEE Transactions on Transportation Electrification

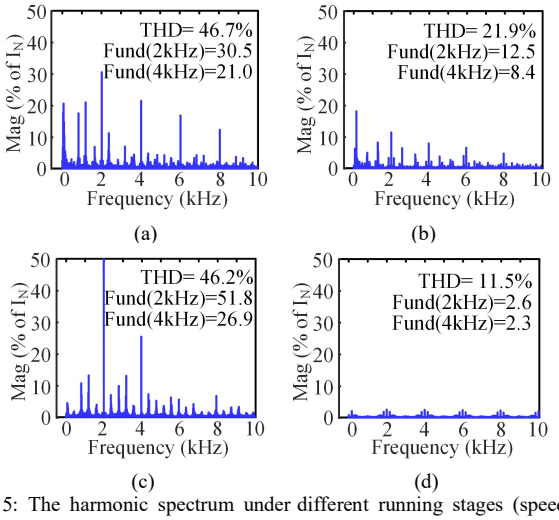

Fig. 5: The harmonic spectrum under different running stages (speed=65 km/h, slope=0‰, passenger flows rate=100%). (a) traction acceleration stage. (b) uniform motion stage. (c) braking stage. (d) stop stage.

T_h, the case temperature T_c and the power loss P_{loss}, the fourth-order Foster model is used to analyze the thermal stress of the DC-link capacitor. Among them, R_{th1}~R_{th4}, C_{th1}~C_{th4}, R_{cond} represent the thermal resistance, heat capacity and heat conduction of each layer in the thermal network, respectively. And the value of thermal parameters can be fitted by the multi-physics model. Fig. 4 shows the thermal stress rise curves of the AL-Cap when the power loss is 50 W and the Film-Cap when the power loss is 20 W with the ambient temperature is 30°C. The rising temperature of Al-Cap is higher than that of Film-Cap. Meanwhile, the temperature rising rate of the Al-Cap is also faster than that of Film-Cap.

III. Multiple Timescale Analysis

A. *Small Timescale of Control Level*

Firstly, in order to characterize the influence of the small timescale of control level on the reliability of the DC-link capacitor, the following sections discuss the effects of the multiple operating conditions and different control methods on the current harmonics of the DC-link capacitor.

a. *Current Harmonic of the Mission Profile*

Different operating stages, speeds, slopes and passenger flows mean different current harmonics of capacitor. Hence, the analysis on current harmonic change for the given mission profile is presented hereunder.

In order to analyze the effects of operating stages on the electrical stress, their total harmonic distortion (THD) is obtained from the harmonic spectrum of the DC-link capacitor current, as shown in Fig. 5, where the output phase current amplitude I_N is used as the fundamental frequency component [9], [14]. Among them, it's worth noting that under different operating stages, the harmonic distribution and the THD value of the DC-link capacitor current have significant differences. In the acceleration and braking stages, the $2f_1$ value (harmonic components at twice the switching frequency), the $4f_1$ value

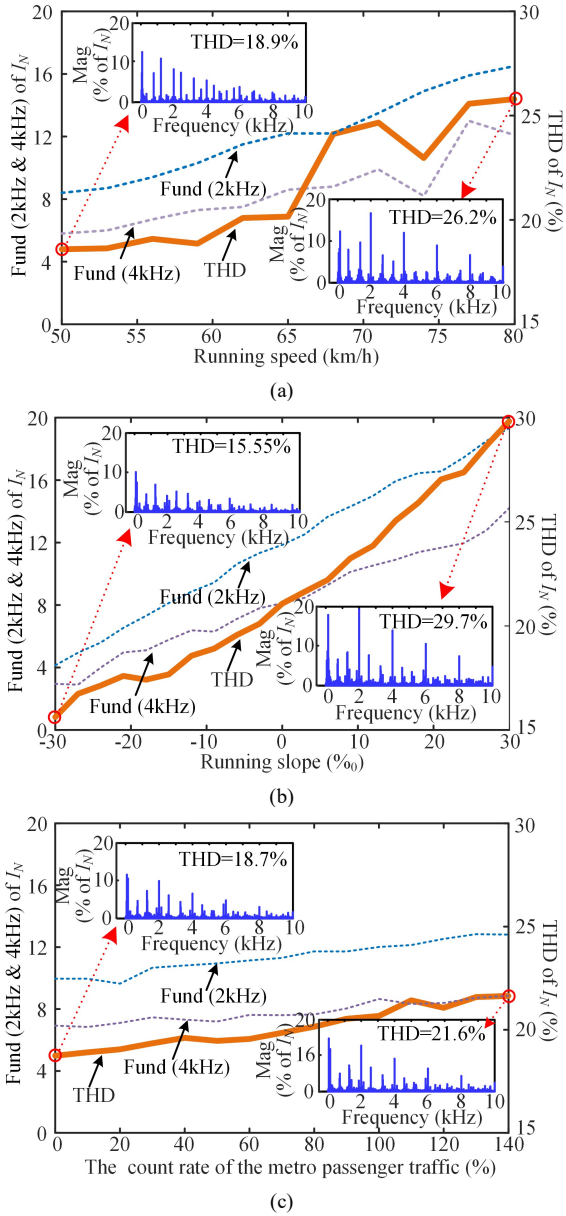

Fig. 6: Harmonic analysis result of the capacitor current (a) under different running speed (slope=0‰, passenger flows rate=100%). (b) under different running slope (speed=65 km/h, passenger flows rate=100%). (c) under different passenger flow rate (speed=65 km/h, slope=0‰)

(harmonic components at four times the switching frequency) and THD value of the capacitor current are much higher than that of the uniform state. Meanwhile, the $2f_1$, $4f_1$ and THD values are the lowest in the stop stage.

The THD for different running speed, different running slopes, different passenger flow rates are obtained from the harmonic spectrum of the DC-link capacitor current is shown in Fig. 6. It can be seen that as the speed, the slope, and the passenger flow rate increases, the $2f_1$ value, $4f_1$ value and THD value of the I_{dc} gradually increases. The THD value at the speed of 80 km/h is about 1.4 times higher than that of 50 km/h. The THD value at the slope of 30‰ is about 2 times of

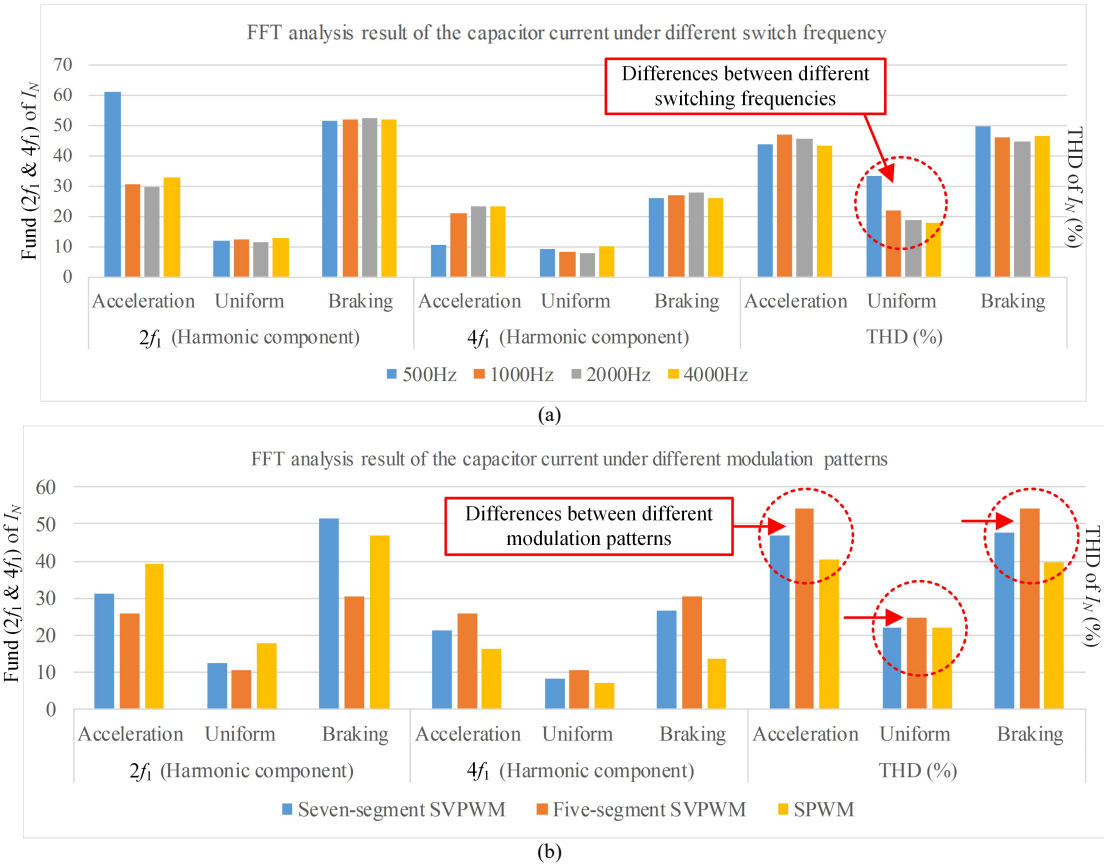

Fig. 7: FFT analysis result of the capacitor current (Operating conditions: the passenger flow rate of = 100%, slope = 0% 0, speed = 65km/h.) (a) under different switch frequency. (b) under different modulation patterns.

the –30‰ slope. Similarly, the THD value at the passenger flow rate of 140% is about 1.15 times of the no-load operation. Based on the above results, it is shown that the influence of the multiple operating conditions on the DC-link capacitor reliability in the small timescale of control level cannot be ignored, especially the running slope and the running speed.

b. The Current Harmonic with Different Control Patterns and Switching Frequencies

Due to the limitations of switching losses and operating efficiency, the low switch frequencies (SF) are usually selected in metro traction drive systems. Fig. 7(a) shows the comparison of SF (500 Hz to 4000 Hz) under the different running stages. Comparing the effects of different SF on the harmonic components of the DC-link capacitor current, the THD value gradually decreases and become stable with the SF increasing. It is worth noting that when the SF is 500 Hz, the THD value is higher than that of others in the uniform motion stage and the proportion of low frequency harmonic content (including the harmonic component $2f_1$) is greater. However, the low frequency harmonics have the greater impact on the reliability of the DC-link capacitor [12].

In order to analyze the influence of different modulation patterns on the DC-link capacitor under the small timescale of control level, the harmonic spectrums of the capacitor current in the Seven-segments SVPWM (7SV), Five-segments SVPWM (5SV), and SPWM (SP) are analyzed. Fig. 7(b) shows the comparison of different modulation patterns with the SF of 1000 Hz. Comparing with the effects of different modulation patterns, the THD value of SV5 is the lowest and the THD value of SPWM is the lowest. In addition, SP contains the highest $2f_1$ and the lowest $4f_1$, while SV5 contains the lowest $2f_1$ and the highest $4f_1$ among the three modulation patterns.

B. Multi-timescale Mission Profile of Electrical Stress

The dynamic working condition ranging from short to long time is experienced in metro traction drive system. In a single route timescale, the startup and shutdown operation, the metro running speed and slope change with the running line. Meanwhile, due to passenger flow, a large stress variation is expected in a given operational period of the day, the working days or the days off for different route timescale, as shown in Fig. 8.

Further, through the drag calculation, the data of running speed v and slope S are converted into speed drag $F(datum)$ and slope drag $F(slope)$, respectively. The $F(total)$ represents the total drag force according to the vehicle performance specification [15] can be defined as:

This article has been accepted for publication in a future issue of this journal, but has not been fully edited. Content may change prior to final publication. Citation information: DOI 10.1109/TTE.2020.2974182, IEEE Transactions on Transportation Electrification

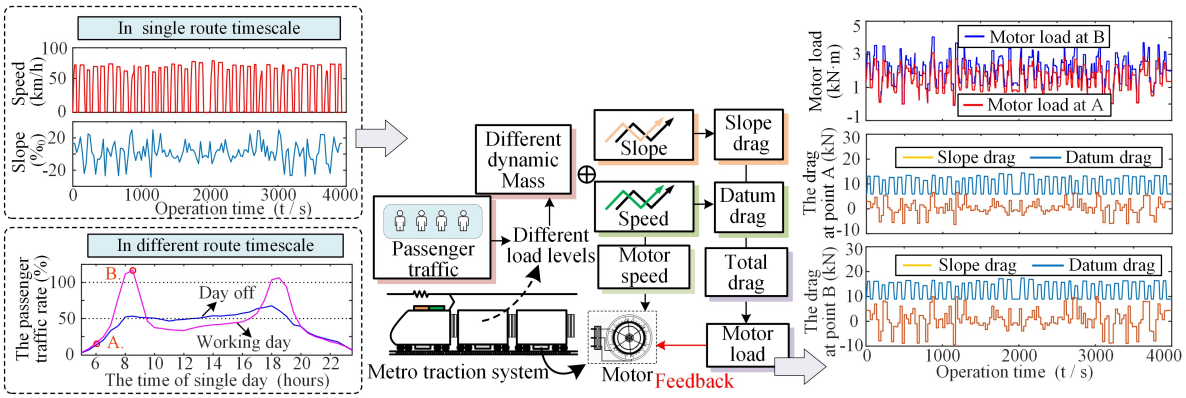

Fig. 8. Block diagram of multi-operating load calculation

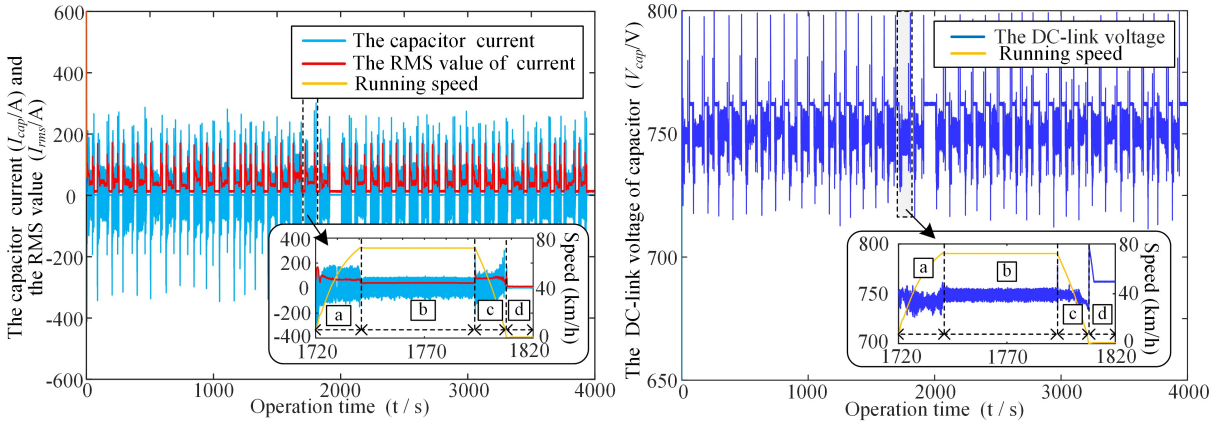

Fig. 9. Simulation results of DC-link capacitor current, RMS value of current, and DC-link voltage in single operating condition

$$\begin{cases} F(slope) = m_{stat} \times s / 1000 \\ F(datum) = 1.98 m_{stat} P_a + 1.334 v^2 \\ F(total) = F(slope) + F(datum) \end{cases} \quad (2)$$

where g, P_a and m_{stat} denote the acceleration of gravity, the passenger traffic rate, and static weight of vehicle, respectively.

Based on this, the running speed v is converted into the motor speed n, and the total drag $F(total)$ is converted into the rated motor torque (motor load) T_e, thereby forming a closed-loop controlled traction drive system [30]:

$$\begin{cases} n = \dfrac{120 a \times v}{3.6 \times \pi \times d \times n_p} \\ T_e = \dfrac{F(total) \times d / 2}{N \times a \times \eta_c} \end{cases} \quad (3)$$

where d, a, n_p, N and η_c denote the wheel diameter, the gear ratio, the number of poles of the motor, the total number of motors and the gear transmission efficiency, respectively.

The calculated load results of the metro passenger traffic rate A and B in the single route timescale as shown in Fig. 8, where point A and point B corresponds to the two data of passenger flows rates. It can be found that the slope drag and speed drag have a considerable influence on the motor load. In addition, because of the increase in passenger capacity, the motor load at point A is higher than the motor load at point B on the overall line.

Fig. 9 shows the simulation result of the DC-link capacitor current, the RMS value of current, and the DC-link voltage. The running time period of the metro from one station to next station can be regarded as one operation cycle. In each operation cycle, the change of capacitor voltage and current can be divided into: a.(traction acceleration stage), b.(uniform motion stage), c.(braking stage) and d.(stop stage). Through the comparison of different load levels, it can be found that when the system is under traction stage and braking stage, the voltage fluctuations and current ripples are more drastic than others.

C. *Multi-Timescale Discrete Calculation of Power Loss*

In order to establish the relationship between the electrical stress and the thermal stress, it is necessary to analyse the power loss generated by the ESR and I_{rms}. According to the equation (1), the overall flow of the capacitor power loss solution is shown in Fig. 10. The I_{rms} signal obtained by the electrical stress test is subjected to Discrete Fourier Analysis (DFT). Meanwhile, a neural network is used to fit the ESR with respect to nonlinear changes of frequency and temperature [31].

The RMS value changes of DC-Link capacitor current according to the electrical stress of different timescales. In

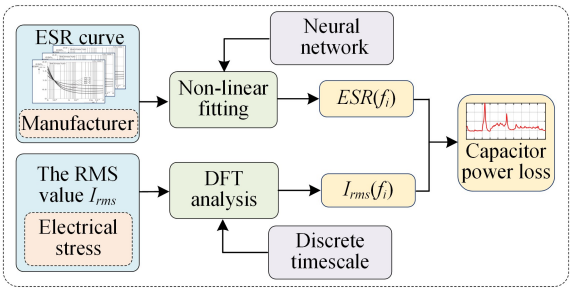

Fig. 10. Solution flow of the capacitor power loss model

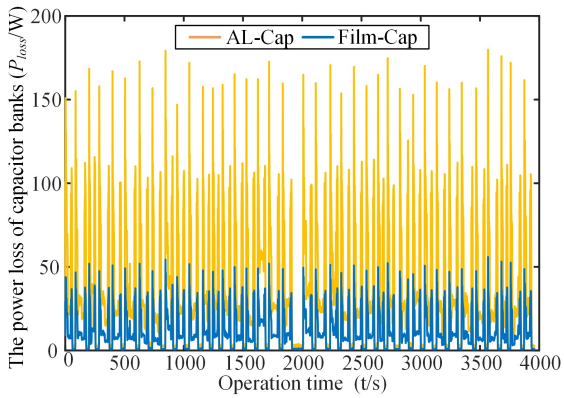

Fig. 11: Simulation results of P_{loss} in the DC-link capacitor

order to represent the change of operation conditions, a discrete timescale DFT analysis model is given:

$$[I_{rms}(f_i,h_k)]=\begin{bmatrix} H(f_1,h_1) & H(f_1,h_2) & \cdots & H(f_1,h_k) \\ H(f_2,h_1) & H(f_2,h_2) & \cdots & \cdots \\ \cdots & \cdots & \cdots & \cdots \\ H(f_i,h_1) & \cdots & \cdots & H(f_i,h_k) \end{bmatrix}[I_{DC}(h_k)] \quad (4)$$

where $H(f_i,h_n)$ represents the ratio of the harmonic of the I_{rms} of nth group when the frequency is f_i to the K group fundamental wave ($I_{DC}(h_n)$), where frequency f_i is taken from 20 Hz to 10 kHz [32].

Based on the above analysis, the dynamic of the power loss of the Film-Cap and the Al-Cap are obtained by nonlinear fitting of the ESR and DFT analysis of I_{rms}, as shown in Fig. 11. The power loss value of the Al-Cap is higher than that of the Film-Cap during the whole operation time. It is observed that the power loss value has a diversity during metro route timescale.

D. *Multi-timescale Mission Profile of Thermal Stress*

Though the instantaneous influence is considered in the mathematical model of hot spot temperature, the time-ordered and continuous of the hot spot temperature needs to be further studied under the multiple timescales. After analyzing the physical properties of the capacitor, it is necessary to superimpose the hot spot temperature to obtain the thermal stress distribution in a longer timescale.

Fig. 12 shows that the capacitors have different rising temperature curves at different power loss values, while the

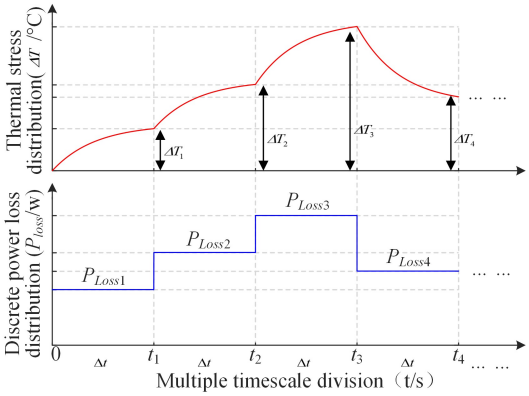

Fig. 12: Power loss and temperature stress dynamic distribution

temperature stress in the next period is affected by the thermal stress of the previous period. It indicates that the hot spot temperature change of the capacitor has time-ordered and continuity, and the rising temperature ΔT of back-to-back time (T_1 and T_2) can be given as:

$$\begin{cases} \Delta T_1 = P_{loss(2)}R_{th}\left(1-e^{\frac{\Delta t}{\tau}}\right) \\ \Delta T_2 = \Delta T_1 \times e^{-\frac{\Delta t}{\tau}} + P_{loss(2)}R_{th}\left(1-e^{\frac{\Delta t}{\tau}}\right) \end{cases} \quad (5)$$

where R_{th} represents the sum of the thermal resistances R_{th1}~R_{th4} of the capacitor, and τ represents the time constant of the full charge of the heat capacity (τ=$R_{th}C_{th}$).

According to the change trend of the thermal stress, the power loss P_{loss} is expressed as the sum from the first segment $P_{loss(1)}$ to the Nth segment $P_{loss(n)}$, thereby obtaining a discrete thermal stress variation model (8) in multiple timescales.

$$\begin{aligned} \Delta T_n &= \begin{Bmatrix} P_{loss(1)}R_{th}e^{-\frac{(n-1)\Delta t}{\tau}} - P_{loss(1)}R_{th}e^{-\frac{n\Delta t}{\tau}} \\ +P_{loss(2)}R_{th}e^{-\frac{(n-2)\Delta t}{\tau}} - P_{loss(2)}R_{th}e^{-\frac{(n-1)\Delta t}{\tau}} \\ + \quad \cdots \quad \cdots \quad + \\ P_{loss(n-1)}R_{th}e^{-\frac{\Delta t}{\tau}} - P_{loss(n-1)}R_{th}e^{-\frac{2\Delta t}{\tau}} \\ +P_{loss(n)}R_{th} - P_{loss(n)}R_{th}e^{-\frac{\Delta t}{\tau}} \end{Bmatrix} \\ &= \sum_{u=1}^{n}\left[P_{loss(u)}R_{th}\left(e^{-\frac{(n-u)\Delta t}{\tau}} - e^{-\frac{(n+1-u)\Delta t}{\tau}}\right)\right] \end{aligned} \quad (6)$$

Fig. 13 shows the original hot spot temperatures (according to mathematical model (1)), the multi-timescale hot spot and case temperatures (according to mathematical models (4)-(6) and physical models). It can be seen that the hot spot temperature changes of the multi-timescale model are smoother than that of the original hot spot temperature, which is in line with the objective law. It indicates that the short-term variation of the thermal stress of the capacitor cannot be ignored in the multi-timescale system. Since the heat capacity of the AL-Cap is smaller than that of the Film-Cap, and ESR of the AL-Cap is larger than that of the Film-Cap, the change

This article has been accepted for publication in a future issue of this journal, but has not been fully edited. Content may change prior to final publication. Citation information: DOI 10.1109/TTE.2020.2974182, IEEE Transactions on Transportation Electrification

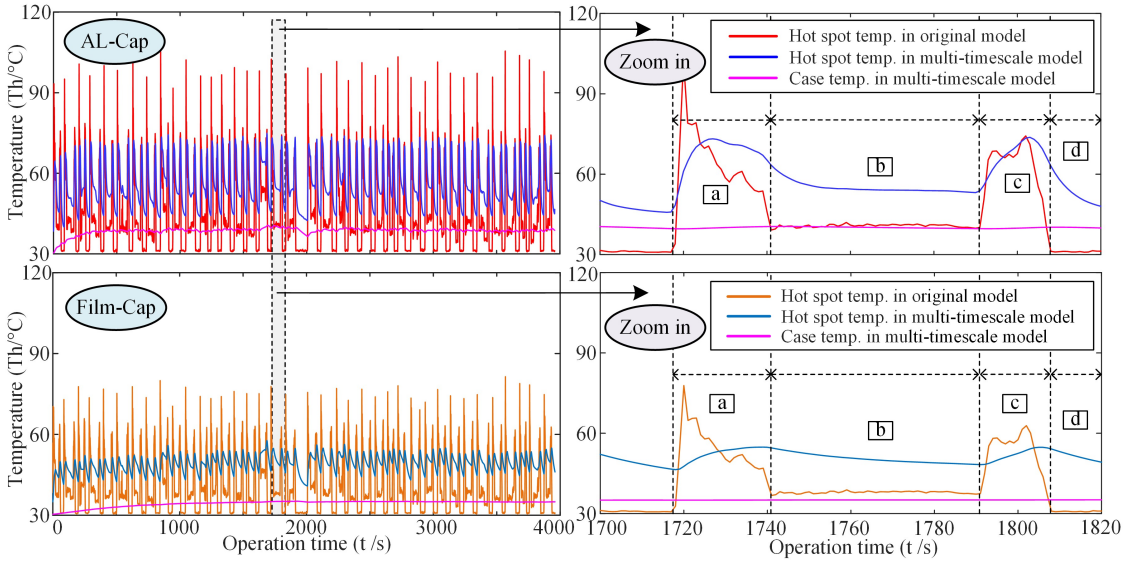

Fig. 13. The thermal model simulation curve of hot spot temperature and case temperature (AL-Cap and Film-Cap)

trend of the AL-Cap hot spot temperature is more obvious and stronger than that of the Film-Cap. Meanwhile, the calculated case temperature reaches stabilize for a period of time.

There is the fact that in the thermal stress analysis, the ambient temperature cannot be neglected. Hence, the influence of ambient temperature on the thermal stress should be analyzed simultaneously. Based on the multi-timescale thermal stress model, the mission profile from the daily running timescale to the long-running timescale is considered, as shown in Fig. 14.

IV. Capacitor Lifetime Estimate

A. *Multiple Timescales Model of the DC-link Capacitor*

After summarizing the multiple timescale analysis of the above electro-thermal stress coupling, it is necessary to further evaluate the lifetime of the capacitor. For AL-cap and Film-Cap, the DC-link capacitor lifetime model is given as [5]:

$$L=L_0\times\left(\frac{V}{V_{cap}}\right)^{-p}\times 2^{\frac{T_0-T_h}{10}} \tag{7}$$

where L, L_0, V, V_{cap}, T_0, and T_h denote the actual lifetime, the rated lifetime, the actual capacitor voltage, the rated capacitor voltage, the rated temperature and actual hot spot temperature, respectively. p is an empirical coefficient that is equal to 4 and 8 in AL-cap and Film-Cap.

Based on the above analysis, the optimal lifetime model of multi-timescale is considered. $T_{h(n)}$ and $L_{s(n)}$ are the smallest units of calculation, which represent the hot spot temperature and lifetime evaluation value of a small timescale discrete point n, respectively. Through the *Miner* linear damage theory [33], the lifetime evaluation values $L_{s(1)}$~$L_{s(n)}$ of the small timescale discrete point n are superimposed to obtain the lifetime estimate $L_{(single)}$ of the single route timescale. Considering the value of the ambient temperature $T_{a(n)}$ and the passenger flow $P_{(n)}$ in single day, the lifetime $L_{(single\text{-}1)}$~$L_{(single\text{-}d)}$ is obtained in different time periods (1~d) respectively, and the lifetime expectancy $L_{(dai)}$ of the daily operation timescale is further obtained. Finally, based on the value of the ambient temperature $T_{a(i)}$ of different dates, taking into account the traffic distribution statistics x and y of the working days and day off, the lifetime expectancy $L_{(com)}$ of the whole lifetime cycle timescale is finally obtained:

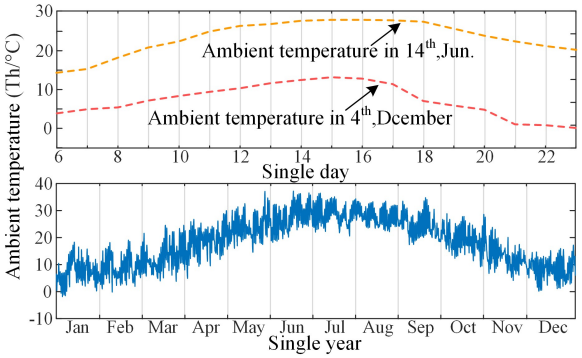

Fig. 14: Mission profile for ambient temperature

*Step:*1 The discrete point timescale:

$$\begin{cases} T_h(n)=\sum_{u=1}^{m}\left[\sum_{i=1}^{k}\left[ESR(f_i)\times\left[H(f_i,h_n)\times I_{DC}(h_n)\right]^2\right]\times R_{th}\left(e^{-\frac{(n-u)\Delta t}{\tau}}-e^{-\frac{(n+1-u)\Delta t}{\tau}}\right)\right]+T_a(n) \\ L_s(n)=L_0\times\left(V_{cap}(n)/V_0\right)^{-q}\times 2^{(T_0-T_h(n))/10} \end{cases} \tag{8}$$

*Step:*2 The single route timescale:

$$L_{(single)}=\frac{1}{\frac{1}{n}\left(\frac{1}{L_{s(1)}}+\frac{1}{L_{s(2)}}+\ldots+\frac{1}{L_{s(n)}}\right)} \tag{9}$$

This article has been accepted for publication in a future issue of this journal, but has not been fully edited. Content may change prior to final publication. Citation information: DOI 10.1109/TTE.2020.2974182, IEEE Transactions on Transportation Electrification

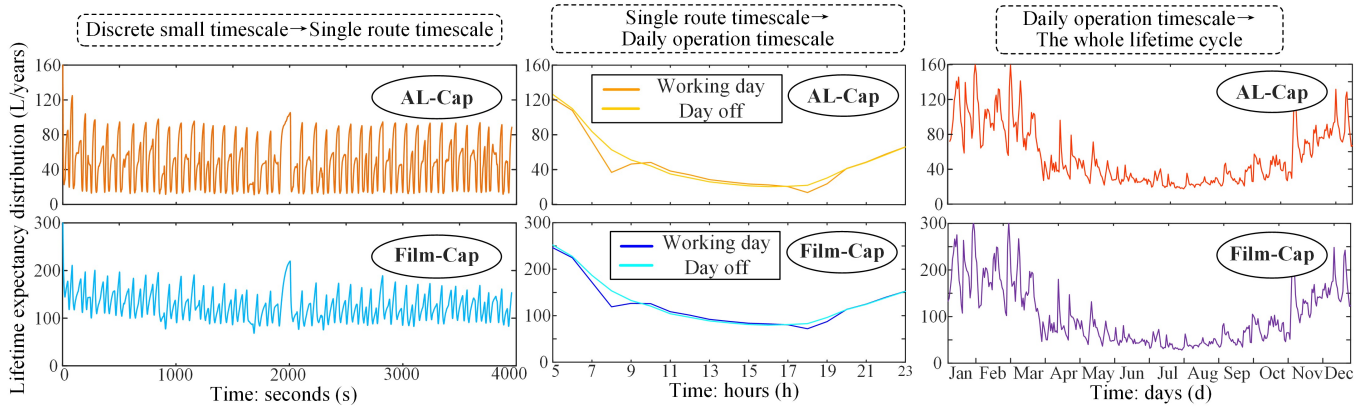

Fig. 15: Calculation results for the lifetime expectancy of AL-cap and Film-Cap

*Step:*3 The daily operation timescale:

$$L_{(dai)}=\frac{1}{\frac{1}{x_1+x_2+\cdots+x_d}\left(\frac{x_1}{L_{(single\text{-}1)}}+\frac{x_2}{L_{(single\text{-}2)}}+\ldots+\frac{x_k}{L_{(single\text{-}d)}}\right)} \quad (10)$$

*Step:*4 The whole lifetime cycle timescale:

$$L_{(com)}=\frac{x+y}{\sum_{i=1}^{x}\left[\frac{1}{L_{(dai-1)}\times 2^{\frac{Ta(i)-Ta(0)}{10}}}\right]+\sum_{i=1}^{y}\left[\frac{1}{L_{(dai-2)}\times 2^{\frac{Ta(i)-Ta(0)}{10}}}\right]} \quad (11)$$

Fig. 15 shows the calculation of the expected lifetime distribution of the DC-link capacitors in multiple timescales models (8)-(11). There are diversities in the impact of different timescales on the reliability of capacitors: Firstly, based on the discrete lifetime expectancy on a small timescale, the mission profile in the route operation corresponds to the single route timescale. The expected lifetime distribution at the time of seconds level has great diversity with the change of train operating conditions, and the result is related to the dynamics and time-ordered of the hot spot temperature. Afterwards, the passenger flow and single-day ambient temperature is reflected in the daily running timescale as well as the seasonal ambient temperature is reflected in the long-running timescale. At the time of the hours and days levels, the lifetime expectancy distribution is directly related to the mission profile of the passenger flow and ambient temperature. Finally, the whole lifetime cycle expectancy of the AL-cap and the Film-cap are 33.89 years and 120.80 years by the calculation model, respectively.

B. *Experimental Verification of the DC-link Capacitor Estimation Results*

The experimental prototype platform for the reliability test about the DC-link capacitor banks is shown in the Fig. 16. In the inverter, the TMS320F28335 digital signal processor is used to implement the closed-loop vector control algorithm. Meanwhile, the flywheel is used to increase the rotary inertia in the motor to simulate the metro operation.

a. *Electrical Stress Experiment of the DC-link Capacitor*

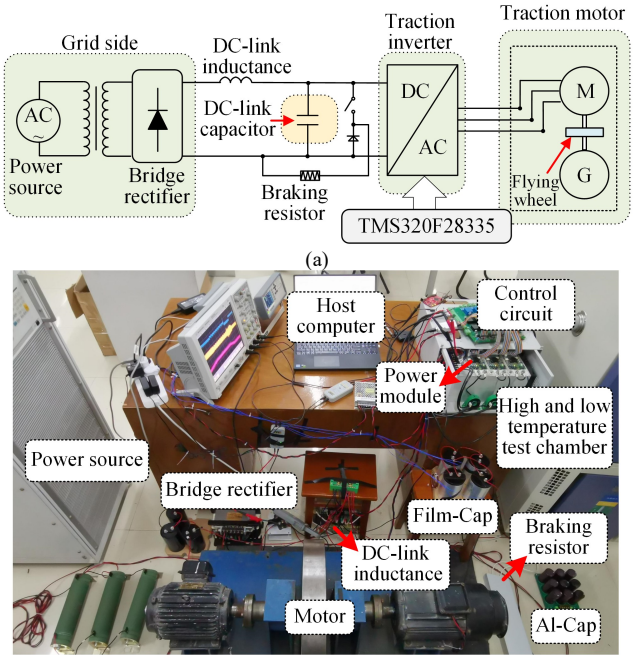

Fig. 16. The experimental prototype platform. (a) System configuration. (b) Photo of experimental test rig.

At the beginning, the SF is set to 1 kHz and the SV7 is used in the inverter control. In order to investigate the different loading conditions impact on the electrical stresses of the DC-link capacitor, the motor speeds of 600, 900, and 1200 r/min are used to emulate the working condition. Fig. 17 shows the DC-link voltage U_{dc}, DC-link capacitor current I_{cap}, and running speed n_d under different motor speeds.

Considering the influence of different control patterns on the electrical stress of DC-link capacitor, which the switching frequencies are further set the range of 500 Hz to 4000 Hz, and the SP and SV5 are used in the inverter control to compare system performance. Fig. 18 and Fig. 19 shows the DC-link voltage, capacitor current and running speed corresponding with different switching frequencies and different modulation patterns.

This article has been accepted for publication in a future issue of this journal, but has not been fully edited. Content may change prior to final publication. Citation information: DOI 10.1109/TTE.2020.2974182, IEEE Transactions on Transportation Electrification

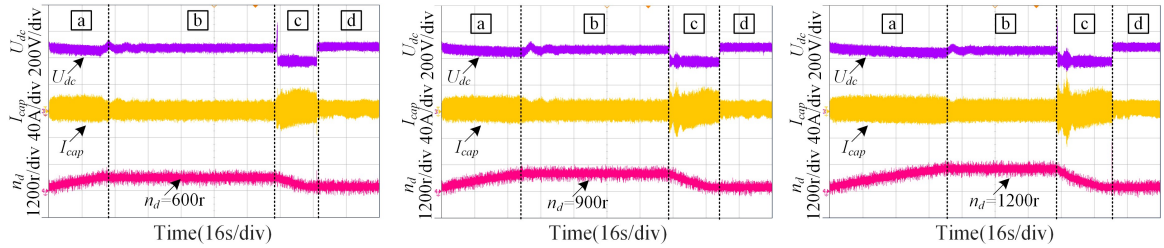

(a) (b) (c)

Fig. 17: Experimental results of DC-link voltage U_{dc}, DC-link capacitor current I_{cap} and running speed n_d (SF = 1000Hz, SV7). (a) Given speed = 600r/min. (b) Given speed = 900r/min. (c) Given speed = 1200r/min.

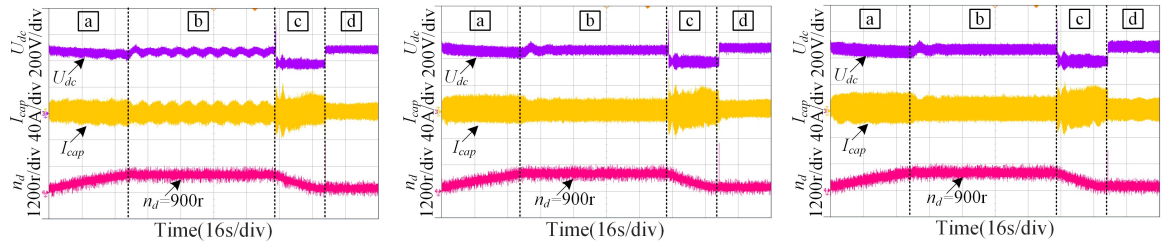

(a) (b) (c)

Fig. 18: Experimental results of DC-link voltage U_{dc}, DC-link capacitor current I_{cap} and running speed n_d (Given speed = 900r/min, SV7). (a) SF = 500Hz. (b) SF = 2000Hz. (c) SF = 4000Hz.

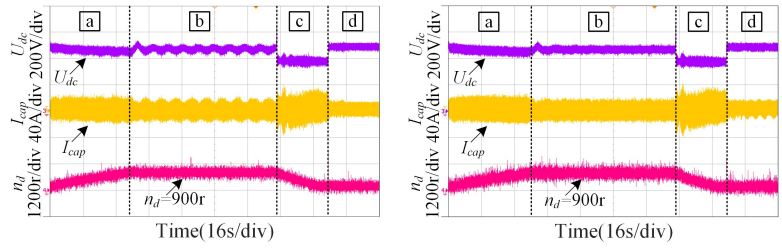

(a) (b)

Fig. 19: Experimental results of DC-link voltage U_{dc}, DC-link capacitor current I_{cap} and running speed (Given speed = 900r/min, SF = 1000Hz). (a) SV5. (b) SP.

From the experimental results, it can be seen that the ripple of the DC-link capacitor current in the acceleration stage and the braking stage is larger than that of the uniform motion stage, while the ripple in the stop stage is the smallest. In addition, under low switching frequency (500 Hz) and SV5 control patterns, the ripple of the capacitor current change greatly.

In order to further quantitatively analyze the effect of electrical stress, the THD value for DC-link capacitor current is shown in Fig. 20, where the time of DC-link capacitor current amplified waveform is 10 ms/div [34]. The THD value of DC-link capacitor in the acceleration stage and the braking stage are approximately 1.5 to 2 times that of uniform motion stage. It is noted that when the low switching frequency (500 Hz) is set or the SV5 modulation mode is used, the THD of I_{cap} in the uniform motion stage are larger. The THD of I_{cap} in the braking stage are smaller than that of SVPWM with the SPWM modulation mode using, and the results are consistent with the simulation model. Furthermore, a spectrum of FFT analysis of a set of experimental data is shown in Fig. 21. The spectrum analysis shows that the high order harmonic components are concentrated at 2 times, 4 times, 6 times, and so on. of the SF, which is consistent with the simulation results in Fig. 5. Of course, the THD of I_{cap} in the experimental acceleration stage is slightly lower than that of the simulation, which may be caused by the high motor power level of the simulation model. Meanwhile, because of the higher low frequency component in the experiment, the THD of I_{cap} of the experimental stop stage is slightly higher than that of the simulation.

b. Thermal Stress Experiment of the DC-link Capacitor

In order to verify the rationality of the thermal stress analysis, the cycle process from acceleration to uniform motion to braking to stop operation is set to simulate the rapid start-stop laws of the metro operation. After waiting for the capacitor case temperature to stabilize, the case temperature of the Al-Cap and Film-Cap is tested by the infrared imager. The temperature rise results of Al-Cap and Film-Cap corresponding to different switching frequencies with the modulation of SV7 are shown in Fig. 22 and Fig. 23 show. Fig. 24 shows the temperature rise results of Al-Cap and Film-Cap with the modulation of SV5 and SP, respectively.

The change trends of rising temperature of Al-Cap and Film-Cap is consistent with the harmonic analysis of capacitor current. The temperature rise of Al-Cap is much higher than

This article has been accepted for publication in a future issue of this journal, but has not been fully edited. Content may change prior to final publication. Citation information: DOI 10.1109/TTE.2020.2974182, IEEE Transactions on Transportation Electrification

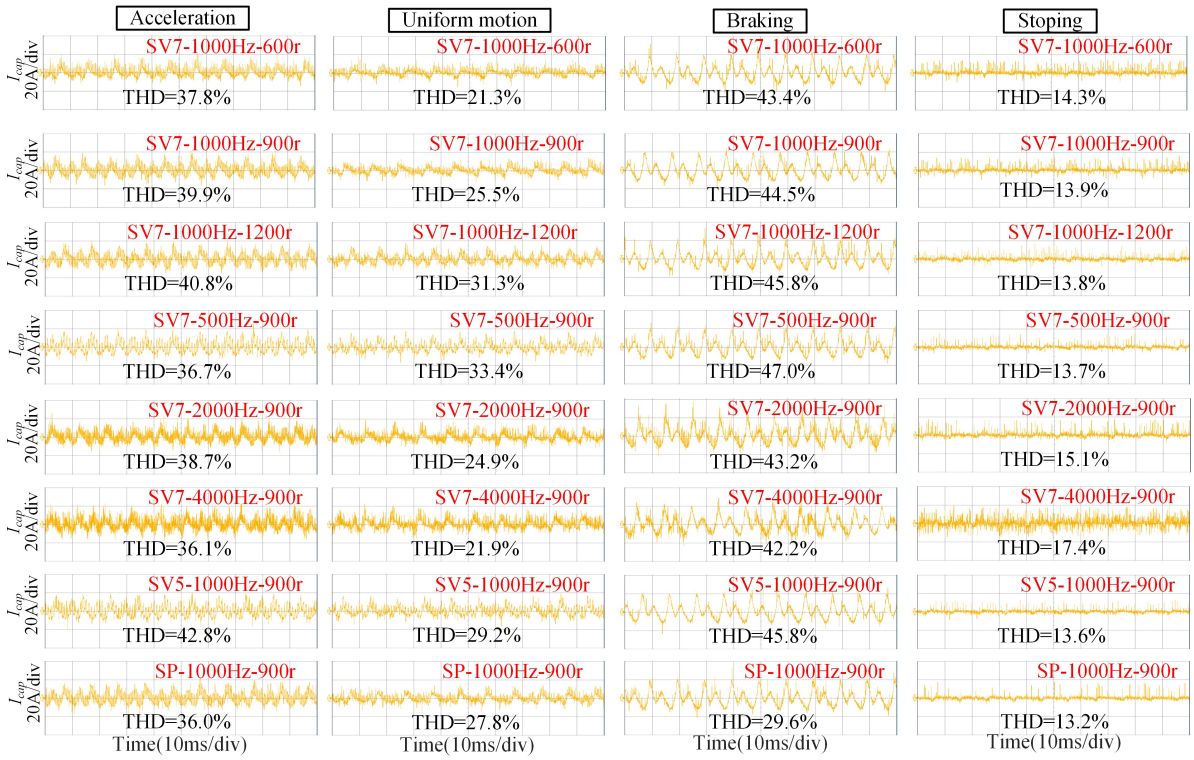

Fig. 20: Experimental amplified waveforms of DC-link capacitor current I_{cap} and the THD value

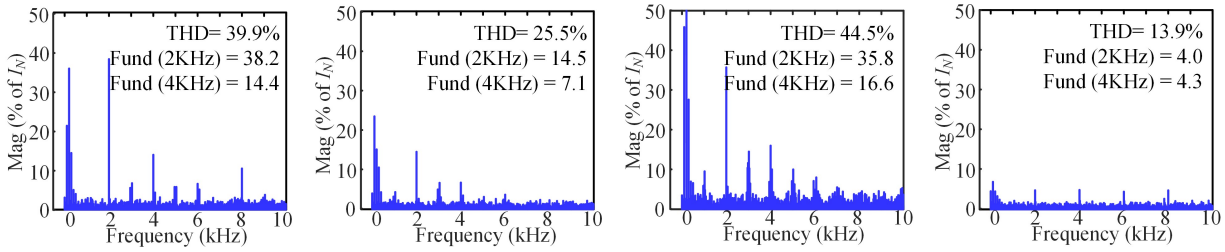

Fig. 21: FFT analysis result of experiment data (Given speed = 900r/min, SF = 1000Hz, SV7). (a) Acceleration. (b) Uniform. (c) Braking. (d) Stop.

that of Film-Cap, which is mainly due to the larger ESR of Al-Cap. Meanwhile, at low switching frequencies, the temperature rise is more pronounced, while the SP modulation has a lower temperature rise.

c. Accelerated Aging Experiment of the DC-link Capacitor

In order to verify the rationality of the lifetime expectancy obtained above, an accelerated aging experiment is performed. Different types of capacitors end-of-life are inconsistent. A typical end-of-life standard for AL-cap is to reduce the C_{cap} by more than 20% and increase the ESR by 2 times. A typical end-of-life standard for Film-Cap is to reduce the C_{cap} by more than 5% and increase the dissipation factor (DF) by 3 times [5].

Therefore, ESR and C_{cap} are used as the monitoring parameters for measuring the lifetime of the AL-cap as well as DF and C_{cap} are used as the monitoring parameters for measuring the lifetime of Film-Cap. The higher ambient temperature T_a (increase 30°C) is set in the high and low temperature test chamber, and the DC-link voltage is increased to 1.2 times. The empirical coefficient p increase with the working conditions of high voltage. The acceleration factor $H_{(acc)}$ of the *Generalized Eyring Relationship* in aging experiment can be expressed as [35], [36]:

$$H_{(acc)} = \left(\frac{V}{1.2V}\right)^{-p} \times 2^{\frac{(T_h+30)-T_h}{10}} \tag{13}$$

In this experiment, the acceleration factors $H_{(acc)}$ of the AL-Cap and the Film-Cap are 23.4 and 49.5, respectively.

The AL-cap and Film-Cap are tested for about 2000 hours and the changes in C_{cap} and ESR or DF are fitted. The value of C_{cap} and ESR or DF are fitted as shown in Fig. 25. According to the failure criteria, the accelerated aging lifetime of the AL-Cap and the Film-Cap is about 4760 hours and 6500 hours,

This article has been accepted for publication in a future issue of this journal, but has not been fully edited. Content may change prior to final publication. Citation information: DOI 10.1109/TTE.2020.2974182, IEEE Transactions on Transportation Electrification

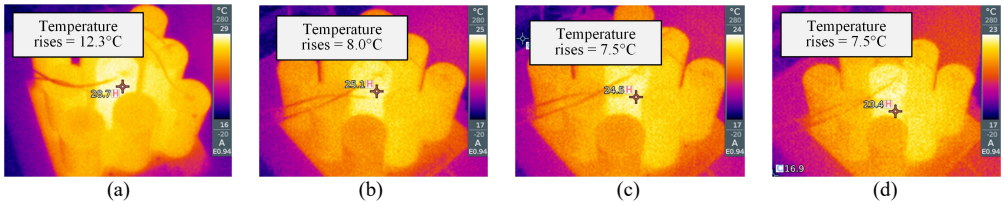

(a) (b) (c) (d)

Fig. 22. Experimental results of case temperature (AL-Cap, SV7). (a) SF = 500Hz. (b) SF = 1000Hz. (c) SF = 2000Hz. (d) SF = 4000Hz.

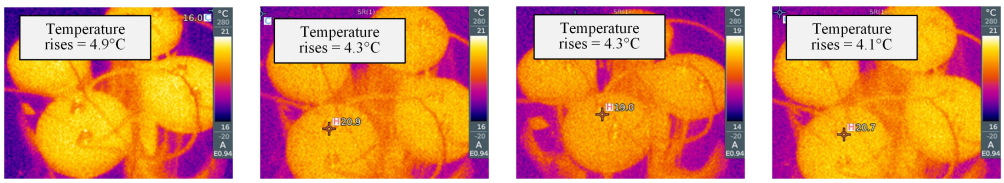

(a) (b) (c) (d)

Fig. 23. Experimental results of case temperature (Film-Cap, SV7). (a) SF = 500Hz. (b) SF = 1000Hz. (c) SF = 2000Hz. (d) SF = 4000Hz.

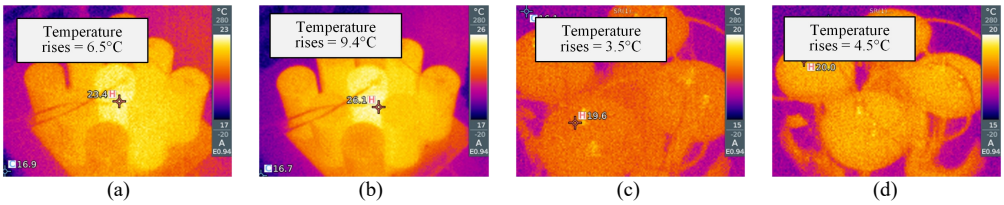

(a) (b) (c) (d)

Fig. 24. Experimental results of AL-Cap and Film-Cap case temperature (SF = 1000Hz). (a) AL-Cap, SP. (b). AL-Cap, SV5. (a) Film-Cap, SP. (b) Film-Cap, SV5.

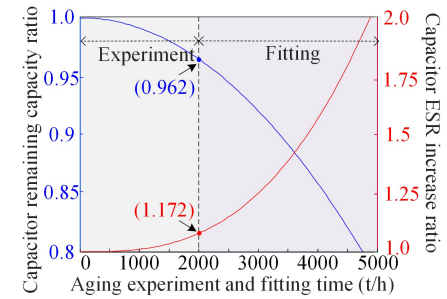

(a)

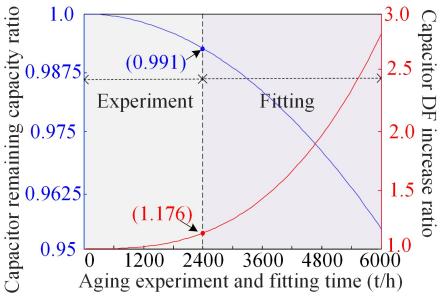

(b)

Fig. 25. Experimental and fitting results of the capacitance and ESR loss. (a) Al-Cap. (b) Film-Cap.

respectively. After multiplying by the acceleration factor $H_{(acc)}$, the Al-Cap has a conversion lifetime of about 20.34 years, and the Film-Cap has a conversion lifetime of about 70.67 years. The experimental results are on the same order of magnitude as the results of multiple timescales model, which shows the rationality of the model. Of course, the experimental results are slightly less than the lifetime expectancy. The high temperature and voltage on the capacitor might be greater than the theoretical value, which may lead to this discrepancy.

C. *Lifetime Evaluation of the DC-link Capacitor Banks*

This paper further discusses the lifetime bottlenecks distribution and the detailed failure variation for AL-Cap and Film-Cap in the operating time by the Weibull distribution. It is assumed that the Weibull shape parameters are invariant in the same failure mode [14]. The variation of the loss rate in the aging experiment are fitted to determine the shape parameter of the Weibull distribution m= 5.06 (Film-Cap) and 5.35 (Al-Cap). Based on the results of the lifetime evaluation, the unreliability distribution of single capacitor can be obtained, and the proportion parameters η of Film-Cap and Al-Cap are 551240 and 160124, respectively.

As shown in Fig. 26, when the unreliability rate reaches 100%, the lifetime of the DC-link capacitor banks of Film-Cap and Al-Cap are **84.4 years and 21.6 years**, respectively. Considering the ratings criteria in railway system [37], when the unreliability rate reaches 5%, the device should be inspected or repaired. At this time, the operation time of capacitor banks of Film-Cap and Al-Cap are **31.9 years and 8.4 years**, respectively.

In order to characterize the influence of parameters and patterns in control timescale on DC-link capacitor reliability, the lifetime bottleneck distribution with different switching frequencies and control patterns is further shown in Fig. 27.

Comparing different control patterns, the lifetime expectancy of DC-link capacitor is highest in SP pattern as well as the lifetime expectancy of DC-link capacitor is lowest

This article has been accepted for publication in a future issue of this journal, but has not been fully edited. Content may change prior to final publication. Citation information: DOI 10.1109/TTE.2020.2974182, IEEE Transactions on Transportation Electrification

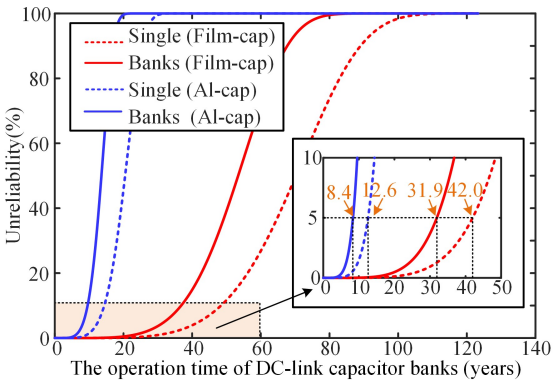

Fig. 26: Unreliability curve of single capacitor and capacitor banks

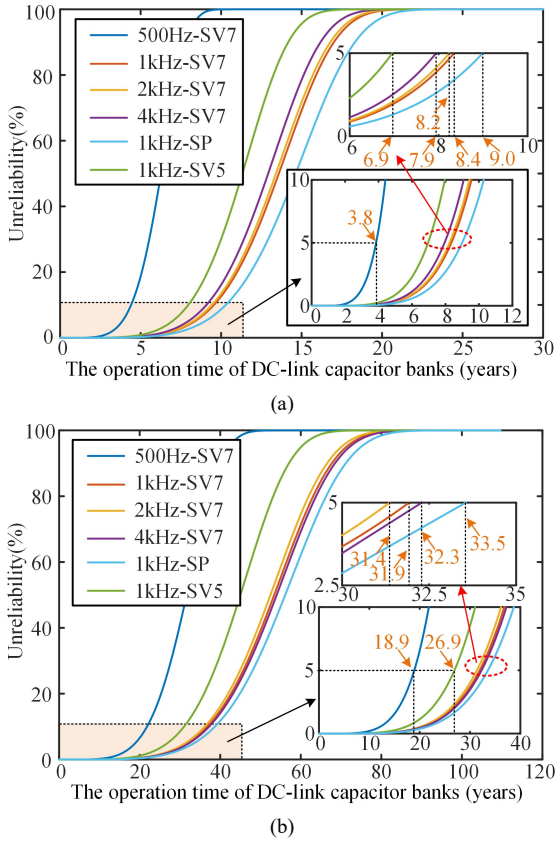

Fig. 27: Unreliability curve with different switching frequencies and control patterns (a)Al-Cap. (b)Film-Cap.

in SV5 pattern. However, because the output voltage of SPWM is 15% lower than the output voltage of SVPWM [38] [39], its practical application in metro traction systems is restricted. It also illustrates the rationality of the application of the SVPWM seven-segments modulation pattern. Comparing different switching frequencies, when the switching frequency is set to 500Hz, the lifetime expectancy is fairly low, only **3.8 years** in Al-Cap and **18.9 years** in Film-Cap (with 5% unreliability rete). With the switching frequency setting from 1k Hz to 4k Hz, the lifetime expectancy of Al-Cap and Film-Cap is distributed in the certain range. In Al-Cap, the lifetime expectancy increases with the switching frequency increasing. In Film-Cap, the lifetime expectancy of SF = 4k Hz is slightly lower than that of 2k Hz and 1k Hz. This result is due to the larger component of the ESR in Film-Cap at low frequencies [5].

VI. Conclusion

This paper describes the reliability evaluation of DC-link capacitors considering the multi-operating condition and complex mission profile in metro drive systems. Based on the analysis of the capacitor electrical stress and thermal stress, a reliability evaluation method of DC-link capacitor with multi-timescale effect is proposed, and the lifetime bottleneck of the DC-link capacitor banks is estimated. The results can provide a reference to use the lower-cost On-condition maintenance (OCM) instead of the scheduled maintenance under complex conditions in the rail transit system. Based on a case study with the proposed specification, it can be concluded that:

1) The electrical signal change of the DC-link capacitor is rapid in the metro traction system. In thermal analysis, the time-ordered and continuity of multiple dynamic hot spot temperature distributions are obtained by electro-thermal coupling. In addition, this calculation combination of the mathematical model, the physical model and the time series is approximate to the real facts in the metro traction system.

2) Reliability analysis of multiple timescales is necessary to the performance of the metro traction drive system. On the different timescale, the lifetime span changes drastically with the dynamics of the running route and complex mission profiles, especially in the single route timescale.

3) The lifetime bottleneck and the failure variation of DC-link capacitor banks under different control modes is obtained by the Weibull distribution. Among them, SV7 shows a moderate impact on the lifetime bottleneck of DC-link capacitor, which is roughly 18% more than that of SV5 and 5% less than that of SV5. Meanwhile, the impact of low switching frequency on the lifetime bottleneck of DC-link capacitors is discussed.

Appendix

The main parameters of metro traction system and the specifications of the AL-Cap and the Film-Cap as well as the parameters of the experimental prototype platform and tested DC-link capacitor are shown in the Table I. Meanwhile, the reliability simulation and analysis results with different switching frequencies and control patterns is presented in the Table II. The THD of capacitor current and capacitor rising temperature in the experimental test is given in the Table III.

This article has been accepted for publication in a future issue of this journal, but has not been fully edited. Content may change prior to final publication. Citation information: DOI 10.1109/TTE.2020.2974182, IEEE Transactions on Transportation Electrification

TABLE I
THE METRO TRACTION SYSTEM AND DC-LINK CAPACITOR PARAMETERS / THE EXPERIMENTAL PLATFORM AND TESTED CAPACITOR PARAMETERS

Metro traction system parameters			**Experimental platform parameters**		
Grid side voltage/frequency	1550V / 50Hz		Grid side voltage/frequency	380V / 50Hz	
DC-link inductance	1.1mH		DC-link inductance	5.4 mH	
Switching frequency	1000Hz		Switching frequency	500/1000/2000/4000Hz	
DC-Link voltage	750V		DC-Link voltage	500V	
Motor rated power/ frequency	190kV•A/ 60.9Hz		Motor rated power/ frequency	3.3 kV•A / 50Hz	
DC-link Capacitor banks parameters			**Prototype DC-link capacitor banks parameters**		
	Film-Cap (4 parallels)	AL-Cap (3 parallels and 3 series)		Film-Cap (4 parallels)	AL-Cap (3 parallels and 3 series)
Capacitance C_{cap}	6mF (1.5mF×4)	6mF	Capacitance C_{cap}	2mF (0.5mF×4)	2mF
Rated voltage V_{cap}	1100V	1200V (400V×3)	Rated voltage V_{cap}	600V	1200V (400V×3)
ESR (1KHz/20°C)	0.5mΩ	3.9mΩ	ESR (1KHz/20°C)	3.0mΩ	25mΩ
Thermal resistance R_{th}	0.92K/W	0.42K/W	Thermal resistance R_{th}	5.6K/W	3.0K/W
Rate load lifetime	100000h (70°C)	6000h (105°C)	Rate load lifetime	100000h (70°C)	6000h (105°C)

TABLE. II
RELIABILITY ANALYSIS RESULTS WITH DIFFERENT SWITCHING FREQUENCIES AND CONTROL PATTERNS

Control pattern	SF (Hz)	THD of I_N (%)				Power loss (W)		Hot spot temp. rise (°C)		Case temp. rise (°C)		Life (year) 100% unreliability		Life (year) 5% unreliability	
		Acceleration	uniform	braking	stopping	Al	Film	Al	Film	Al	Film	Al	Film	Al	Film
SV7	500	43.7%	33.1%	49.5%	11.6%	72.93	22.53	34.44	21.10	12.67	5.19	15.64	71.62	3.8	18.9
	1000	46.7%	21.9%	46.2%	11.5%	51.99	16.78	21.66	14.30	8.24	4.03	33.89	120.80	8.3	31.9
	2000	45.4%	18.7%	44.7%	11.8%	48.04	17.44	21.70	14.54	8.25	4.08	33.45	118.68	8.2	31.4
	4000	43.1%	17.9%	46.6%	12.6%	53.82	18.11	21.83	14.11	8.38	3.47	32.24	122.18	7.9	32.3
SV5	1000	54.3%	24.8%	54.1%	12.3%	52.72	17.48	24.80	16.71	9.46	4.68	28.24	101.80	6.9	26.9
SP	1000	40.2%	22.0%	39.5%	11.5%	48.91	15.46	21.02	13.62	8.03	3.83	36.50	126.96	9.0	33.5

The power loss, the hot spot temperature and the case temperature are the average values in the single route timescale.

TABLE. III
THE RESULTS IN THE EXPERIMENTAL TEST

Control patterns	SF (Hz)	Exp. (THD)				Case rising temp. (/°C)	
		A	B	C	D	Al-Cap	Film-Cap
SV7	500	36.7%	33.4%	47.0%	13.7%	12.3	4.9
	1000	39.9%	25.5%	44.5%	13.9%	8.0	4.3
	2000	38.7%	24.9%	43.2%	15.1%	7.5	4.3
	4000	36.1%	21.9%	42.2%	17.4%	7.5	4.1
SV5	1000	42.8%	29.2%	45.8%	13.6%	9.4	4.5
SP	1000	36.0%	27.8%	31.6%	13.2%	6.5	3.5

REFERENCES

[1] K. Ma, M. Liserre, F. Blaabjerg, and T. Kerekes, "Thermal loading and lifetime estimation for power device considering mission profiles in wind power converter," *IEEE Trans. Power Electron*., vol. 30, no. 2, pp. 590-602, Feb. 2015.

[2] H. Wang, M. Liserre, and F. Blaabjerg, "Toward reliable power electronics: challenges, design tools, and opportunities," *IEEE Ind. Electron. Mag.*, vol. 7, no. 2, pp. 17-26, Jun. 2013.

[3] H. Wang, H. Wang, G. Zhu, and F. Blaabjerg, "An Overview of Capacitive DC-Links-Topology Derivation and Scalability Analysis," *IEEE Trans. on Power Electron.*, vol. 35, no. 2, pp. 1805-1829, Feb. 2020.

[4] B. Gou, X. Ge, S. Wang, X. Feng, J. B. Kuo, and T. G. Habetler, "An open-switch fault diagnosis method for single-phase pwm rectifier using a model-based approach in high-speed railway electrical traction drive system," *IEEE Trans. Power Electron.*, vol. 31, no. 5, pp. 3816-3826, May 2016.

[5] H. Wang and F. Blaabjerg, "Reliability of capacitors for DC-link applications in power electronic converters–an overview," *IEEE Trans. Ind. Appl.*, vol. 50, no. 5, pp. 3569-3578, Sep./Oct. 2014.

[6] K. Urata and T. Shimizu, "Temperature estimation of aluminum electrolytic capacitor under actual circuit operation," in *2018 Int. Power Electron. Conf. (IPEC-Niigata 2018 -ECCE Asia)*, Niigata, 2018, pp. 302-308.

[7] B. Sun, X. Fan, C. Qian, and G. Zhang, "Pof-simulation-assisted reliability prediction for electrolytic capacitor in led drivers," *IEEE Trans. Ind. Electron.*, vol. 63, no. 11, pp. 6726-6735, Nov. 2016.

[8] M. Hinkkanen and J. Luomi, "Induction motor drives equipped with diode rectifier and small DC-Link capacitance," *IEEE Trans. Ind. Electron.*, vol. 55, no. 1, pp. 312-320, Jan. 2008.

[9] H. Wen, W. Xiao, X. Wen, and P. Armstrong, "Analysis and Evaluation of DC-Link Capacitors for High-Power-Density Electric Vehicle Drive Systems," *IEEE Trans. Veh. Technol.*, vol. 61, no. 7, pp. 2950-2964, Sep., 2012.

[10] M. Horák and P. Mach, "Study of thermal ageing of polypropylene film capacitors," in *2015 IEEE 21st Int. Symp. for Des. and Technol. in Electron. Packag. (SIITME)*, Brasov, 2015, pp. 57-60.

[11] Z. Li *et al*., "Lifetime prediction of metallized film capacitors based on capacitance loss," *IEEE Trans. Plasma Sci.*, vol. 41, no. 5, pp. 1313-1318, May 2013.

[12] H. Wang, P. Davari, H. Wang, D. Kumar, F. Zare, and F. Blaabjerg, "Lifetime estimation of DC-link capacitors in adjustable speed drives under grid voltage unbalances," *IEEE Trans. Power Electron.*, vol. 34, no. 5, pp. 4064-4078, May 2019.

[13] D. Zhou, H. Wang, and F. Blaabjerg, "Mission profile based system-level reliability analysis of DC/DC converters for a backup power application," *IEEE Trans. Power Electron.*, vol. 33, no. 9, pp. 8030-8039, Sep. 2018.

[14] D. Zhou, Y. Song, Y. Liu, and F. Blaabjerg, "Mission profile based reliability evaluation of capacitor banks in wind power converters," *IEEE Trans. Power Electron.*, vol. 34, no. 5, pp. 4665-4677, May 2019.

[15] A. Sangwongwanich, Y. Yang, D. Sera, and F. Blaabjerg, "Mission Profile-Oriented Control for Reliability and Lifetime of Photovoltaic Inverters," *IEEE Trans. on Ind. Appl.*, vol. 56, no. 1, pp. 601-610, Jan.-Feb. 2020.

[16] J. Ding, P. Zhang, and J. Li, "Fatigue life prediction of IGBT module for metro vehicle traction converter based on traction calculation," in *2015 IEEE 11th Int. Conf. on Power Electron. and Drive Syst.*, Sydney, NSW, 2015, pp. 1116-1121.

[17] J. Rajmond and P. Dan, "Thermal modeling of through hole capacitors," in *2012 IEEE 18th Int. Symp. for Des. and Technol. in Electron. Packag. (SIITME)*, Alba Iulia, 2012, pp. 227-232.

[18] H. Wang and H. Wang, "Capacitive DC links in power electronic systems-reliability and circuit design," *Chinese J. of Elect. Eng.*, vol. 4, no. 3, pp. 29-36, Sep. 2018.

[19] H. Wang and H. Wang, "An analytical circuit based nonlinear thermal model for capacitor banks," *Microelectronics Rel.*, vol. 88, pp. 524-527, Jun. 2018.

[20] Y. Wu and X. Du, "A VEN condition monitoring method of DC-link capacitors for power converters," *IEEE Trans. Ind. Electron.*, vol. 66, no. 2, pp. 1296-1306, Feb. 2019.

[21] P. Freiburger, "Transient thermal modeling of aluminum electrolytic capacitors under varying mounting boundary conditions," in *2015 21st Int. Workshop on Thermal Investigations of ICs and Systems (THERMINIC)*, Paris, 2015, pp. 1-5.

[22] Z. Na, "A study of electrolytic capacitor's thermal conductivity, behavior and measurement," in *2016 22nd International Workshop on Thermal Investigations of ICs and Syst. (THERMINIC)*, Budapest, 2016, pp. 315-318.

[23] Z. Li *et al*., "Temperature rise of metallized film capacitors in repetitive pulse applications," *IEEE Trans. Plasma Sci.*, vol. 43, no. 6, pp. 2038-2045, Jun. 2015.

[24] W. Sarwar, M. Marinescu, N. Green, N. Taylor, and G. Offer, "Electrochemical double layer capacitor electro-thermal modelling," *J. of Energy Storage*, 2016, 5: 10-24.

[25] I. Colak, S. Sagiroglu, M. Yesilbudak, E. Kabalci, and H. I. Bulbul, "Multi-time series and time scale modeling for wind speed and wind power forecasting part I: Statistical methods, very short-term and short-term applications," in *2015 Int. Conf. on Renewable Energy Res. and Applications (ICRERA)*, Palermo, 2015, pp. 209-214.

[26] R. Billinton and D. Huang, "Incorporating wind power in generating capacity reliability evaluation using different models," *IEEE Trans. Power Syst.*, vol. 26, no. 4, pp. 2509-2517, Nov. 2011.

[27] B. Dong, J. He, and X. Fang, "The parameter sensitivity study of small time scale crack growth model," in *2015 Prognostics and Syst. Health Manage. Conf. (PHM)*, Beijing, 2015, pp. 1-4.

[28] K. Ma, M. Liserre, F. Blaabjerg, and T. Kerekes, "Thermal Loading and Lifetime Estimation for Power Device Considering Mission Profiles in Wind Power Converter," *IEEE Trans. Power Electron.*, vol. 30, no. 2, pp. 590-602, Feb. 2015.

[29] H. Wang, X. Ge, and Y. Liu, "An active damping stabilization scheme for the suppression of the DC-link oscillation in metro traction drive system," *IEEE Trans. Ind. Appl.*, vol. 54, no. 5, pp. 5113-5123, Sep./Oct. 2018.

[30] M. Wang, B. Kou, and X. Zhao, "Analysis of energy consumption characteristics based on simulation and traction calculation model for the CRH electric motor train units," in *2018 21st Int. Conf. on Elect. Mach. and Syst. (ICEMS)*, Jeju, 2018, pp. 2738-2743.

[31] B. Yao, X. Ge , L. Shu, H. Wang, Z. Hu, and B. Gou. "Life estimation of DC-link capacitor in multi-operating traction drive system," *in 2019 IEEE 10th Int. Conf. on Power Electron. (ICPE-ECCE Asia)*, Busan, 2019, pp. 2743-2748.

[32] K. Laadjal, M. Sahraoui, A. J. M. Cardoso, and A. M. R. Amaral, "Online estimation of aluminum electrolytic-capacitor parameters using a modified Prony's method," *IEEE Trans. Ind. Appl.*, vol. 54, no. 5, pp. 4764-4774, Sep./Oct. 2018.

[33] Todinov M T. "Necessary and sufficient condition for additivity in the sense of the Palmgren–Miner rule,". *Comput. Mater. Sci.*, 2001, 21(1): 101-110.

[34] H. Wang, Y. Liu, and H. Wang, "On the Practical Design of a Two-Terminal Active Capacitor," *IEEE Trans. on Power Electron.*, vol. 34, no. 10, pp. 10006-10020, Oct. 2019.

[35] BS EN 61881-1:2011:Raliway applications-rolling stock equipement-capacitors for power electronics

[36] E. Redondo-Iglesias, P. Venet, and S. Pelissier, "Global model for self-discharge and capacity fade in lithium-ion batteries based on the generalized eyring relationship," *IEEE Trans. Veh. Technol.*, vol. 67, no. 1, pp. 104-113, Jan. 2018.

[37] GB/T Standard Voltages, GB/T 21562.2, 2015. Railway applications-Specification and demonstration of reliability, availability, maintainability and safety (RAMS)-Rart 2: Guide to the application for safety.

[38] D. Ronanki and S. S. Williamson, "A Simplified Space Vector Pulse Width Modulation Implementation in Modular Multilevel Converters for Electric Ship Propulsion Systems," *IEEE Trans. Transport. Electrific.*, vol. 5, no. 1, pp. 335-342, Mar. 2019.

[39] Y. Ruan, Chen Weijun. Motion Control System. Beijing: Tsinghua University Press, 2007

Bo Yao received the B.Eng. degrees in electrical engineering from Southwest Jiaotong University (SWJTU), Chengdu, China, in 2016. He is currently working toward the M.Eng. degree in electrical engineering at the Southwest Jiaotong University, Chengdu, China.

His research interest is the reliability evaluation of power electronic devices in traction transmission system.

Mr. Yao was a recipient of the Best Paper Award of International Conference on Electrical Machines and Systems (ICEMS) in 2019.

Xinglai Ge (M'15) received the B.S., M.S., and Ph.D. degrees in electrical engineering from Southwest Jiaotong University (SWJTU), Chengdu, China, in 2001, 2004, and 2010, respectively. He is currently a Full Professor in the School of Electrical Engineering, Southwest Jiaotong University and a Vice Director of Department of Power Electronics and Power Drive.

From July to August of 2012, he was a visiting scholar at George Mason University, VA, USA. From October 2013 to October 2014, he was a visiting scholar at the School of Electrical and Computer Engineering, Georgia Institute of Technology, Atlanta, GA, USA. He is the author and co-author of more than 60 technical papers

His research interests include stability analysis and control of electrical traction system, fault diagnosis and hardware-in-the-loop simulation of traction converter and motor drive system.

Huimin Wang (S'17) received the B.Eng. degrees in electrical engineering from Southwest Jiaotong University (SWJTU), Chengdu, China, in 2016. He is currently working toward the Ph.D. degree in electrical engineering at the Southwest Jiaotong University, Chengdu, China.

His research interests include linear induction motor drive system and its speed-sensorless control.

Mr. Wang was a recipient of the Best Paper Award of IEEE Transportation Electrification Conference and EXPO Asia-Pacific (ITEC Asia-Pacific) in 2019.

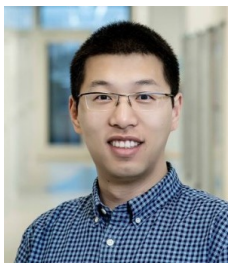

Haoran Wang (S'15-M'18) received the B.S. and M.S. degrees in control science and engineering from Wuhan University of Technology, Wuhan, China, in 2012 and 2015, respectively, and the Ph.D. degree in power electronics from Center of Reliable Power Electronics (CORPE), Aalborg University, Aalborg, Denmark, in 2018, where he is currently an Assistant Professor. From Jul. 2013 to Sep. 2014, he was research assistant with the Department of Electrical Engineering, Tsinghua University, Beijing, China. He was a Visiting Scientist with the ETH Zurich, Switzerland, from Dec. 2017 to Apr. 2018.

His research interests include capacitors in power electronics, reliability of power electronic systems, and multi-objective life-cycle performance optimization of power electronic systems.

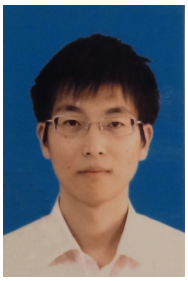

Dao Zhou (S'12, M'15, SM'18) received the B.S. from Beijing Jiaotong University, Beijing, China, in 2007, the M. S. from Zhejiang University, Hangzhou, China, in 2010, and the Ph.D. from Aalborg University, Aalborg, Denmark, in 2014, all in electrical engineering. Since 2014, he has been with Department of Energy Technology, Aalborg University, where currently he is an Assistant Professor. His research interests include modeling, control, and reliability of power electronics in renewable energy application.

Dr. Zhou received the Renewable and Sustainable Energy Conversion Systems of the IEEE Industry Applications Society First Prize Paper Award in 2015, and Best Session Paper at Annual Conference of the IEEE Industrial Electronics Society (IECON) in Austria in 2013.

Bin Gou (S'14–M'17) received the B.S. and Ph.D. degrees in electrical engineering from Southwest Jiaotong University, Chengdu, China, in 2010 and 2016. From 2014 to 2015, he was a Visiting Student at the School of Electrical and Computer Engineering, Georgia Institute of Technology, Atlanta, GA, USA. From 2017 to 2020, he was a Research Fellow in the Rolls-Royce @ NTU Corporate Laboratory, Nanyang Technological University, Singapore. He is with the School of Electrical Engineering, Southwest Jiaotong University, Chengdu, China.

His research interest includes data-analytics for fault diagnosis and health management of power drive and energy system.